## Factors underlying the perturbation resistance of the trunk in the first part of a lifting movement

van der Burg, J.C.E.; Casius, L.J.R.; Kingma, I.; van Dieen, J.H.; van Soest, A.J.

***published in***
Biological Cybernetics
2005

***DOI (link to publisher)***
10.1007/s00422-005-0583-x

***document version***
Publisher's PDF, also known as Version of record

Biol Cybern (2005) 93: 54–62
DOI 10.1007/s00422-005-0583-x

ORIGINAL PAPER

Biological Cybernetics

J.C.E. van der Burg · L.J.R. Casius · I. Kingma · J.H. van Dieën · A.J. van Soest

# Factors underlying the perturbation resistance of the trunk in the first part of a lifting movement

Received: 30 August 2004 / Accepted: 4 May 2005 / Published online: 6 July 2005


**Abstract** In the first part of lifting movements, the trunk movement is surprisingly resistant to perturbations. This study examined which factors contribute to this perturbation resistance of the trunk during lifting. Three possible mechanisms were studied: force-length-velocity characteristics of muscles, the momentum of the trunk as well as the effect of passive extending of the elbows. A forward dynamics modelling and simulation approach was adopted with two different input signals: (1) stimulation of Hill-type muscles versus (2) net joint moments. Experimental data collected during an unperturbed lifting movement were used as a reference, which a simulated lifting movement had to resemble. Subsequently, the simulated lifting movement was perturbed by applying 10 kg extra mass at the wrist (both before and after lift-off and with/without a fixed elbow), without modifying the input signals. The momentum of the trunk appeared to be insufficient to explain the perturbation resistance of trunk movements as found experimentally. In addition to the momentum of the trunk, the force-length-velocity characteristics of the muscles are necessary to account for the observed perturbation resistance. Initial extension of the elbow due to the mass perturbation delayed the propagation of the load to the shoulder. However, this delay is reduced due to the impedance at the elbow provided by the characteristics of muscles spanning the elbow. So, the force-length-velocity characteristics of the muscles spanning the elbow joint increase the perturbation at the trunk.

J.C.E. van der Burg (✉) · L.J.R. Casius
I. Kingma · J.H. van Dieën · A.J. van Soest
Institute for Fundamental and Clinical
Human Movement Sciences,
Faculty of Human Movement Sciences,
Vrije Universiteit Amsterdam,
Van der Boechorststraat 9,
1081 Amsterdam,
The Netherlands
E-mail: P_van_der_Burg@fbw.vu.nl
Tel.: +31-20-5988457
Fax: +31-20-5988529

**Keywords** Lifting · Forward simulation · Muscle dynamics · Perturbations

## 1 Introduction

Lifting movements are little affected when the mass to be lifted is not as expected. Given that subjects anticipate the mass they are going to lift (de Looze et al. 2000), it might be expected that in response to, for example, an unexpectedly increased object mass, the lifting movement is disturbed to the extent that subjects fall forward. Surprisingly, van der Burg and van Dieën (2000, 2001b) found that subjects were able to successfully lift an object that was 10 kg heavier than what they expected even though the trunk muscle activity as measured in surface EMG signals was not adapted until 100 ms after the perturbation occurred. This was seen both when the added mass was effective from the start of the lifting movement and when it was added after lift-off. As an additional 125–135 ms lag after changes in trunk EMG exists before the resulting muscle force is effective (van Dieen et al. 1991), it is remarkable that the large mechanical perturbations imposed by the 10 kg increase in object mass did not severely disrupt the kinematics of the trunk during the first 250 ms of the lifting movement (Fig. 1).

A mechanism that may explain the resistance to perturbations is the momentum of the head–trunk segment prior to lift-off. The momentum caused by the upward velocity of the upper body might be sufficient to lift a heavier object only by slowing down the lifting movement.

Another possible mechanism that may explain the perturbation resistance of the trunk in the first part of the lifting movement is the interaction between segments, as the perturbation is not directly applied at the trunk. In the lifting task especially the elbow could help to postpone the perturbation to the trunk by extending (or flexing more slowly) immediately after the perturbation due to the unexpectedly high mass.

A third mechanism that can explain the perturbation resistance is formed by the force-length-velocity characteristics

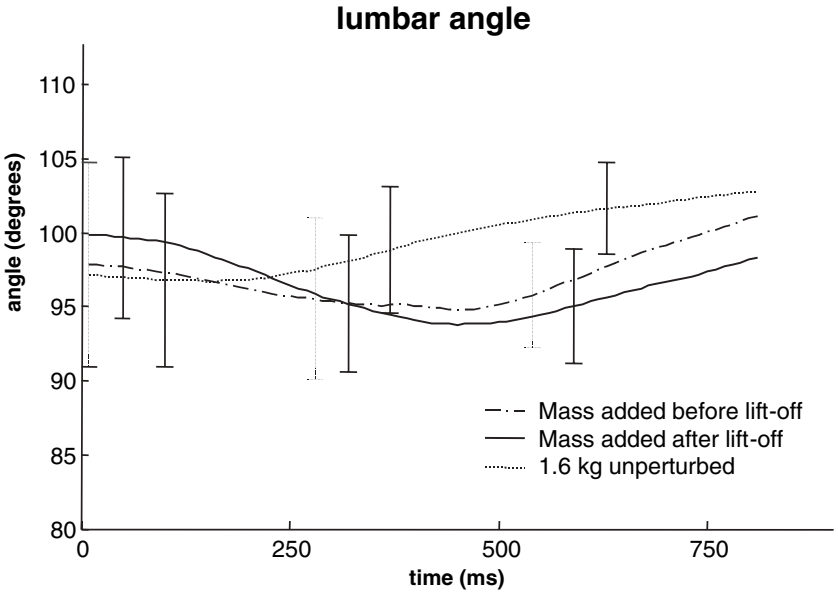


**Fig. 1** Time series of the average lumbar angle for ten subjects after a 10 kg perturbation was applied [adopted from van der Burg and van Dieën (2001b)]. The *dashed-dotted line* represents the condition in which the added mass was effective from the start of the lifting movement, the *solid line* represents the condition in which the mass was added after lift-off, and the *dotted line* represents the unperturbed lifting movement. Note that in the first 250 ms, the deviations from the unperturbed condition are small

of skeletal muscles, which could be a first line of defence against external perturbations (e.g., van Soest and Bobbert 1993; Seyfarth et al. 2001; Wagner and Blickhan 2003). These properties give rise to an instantaneous adaptation of muscle force in response to a disturbed movement, in absence of any change of the neural input to the muscle. Three aspects of muscle physiology contribute to this behavior. First of all, the force–velocity relationship implies that when a muscle is stretched or contracts more slowly, it will produce more force and thereby oppose this stretch. Second, the force–length relationship of muscle that results from length dependent myofilament overlap is such that for any muscle that is below optimum length, a disturbance of length will lead to a change in force that opposes the length change. Third, the length-dependent [$Ca^{2+}$] sensitivity of the binding site of troponine is such that a length perturbation leads to a change in force that opposes the length perturbation (Hatze 1981b; Stienen et al. 1985; Kistemaker et al. 2005, in press).

The aim of this study was to clarify which factors contribute to the initial insensitivity of the trunk movement to a perturbation during lifting as observed experimentally. Three possible mechanisms were studied: force-length-velocity characteristics of muscles, the momentum effect of the trunk as well as the effect of allowing extension of the elbows. As this issue is difficult if not impossible to address experimentally, the goal was pursued by means of forward simulations.

## 2 Methods

In order to assess the contribution of the three factors mentioned to the initial insensitivity of the trunk movement to a perturbation during lifting, forward dynamics simulations of a whole body lifting movement were performed. Calculations were done using two open-loop controlled models. Both models make use of the same skeletal system. In the first model, the skeleton was actuated by muscles with force-length-velocity characteristics (STIM-model). In the second model, the force-length-velocity characteristics had been removed, and the skeleton was driven by net joints moments (MOM-model). To asses the effects of elbow movement, a model in which no elbow movement was allowed and a model with no restriction on elbow movements were run with both STIM and MOM control. Thus, in total, four different models were used: STIM model with fixed elbow, STIM model with free elbow, MOM model with fixed elbow and MOM model with free elbow.

### 2.1 Model of the musculo-skeletal system

The skeleton consisted of a 2D-chain of seven segments, representing the feet, lower legs, upper legs, pelvis, trunk and head, upper arms, and forearms (see Table 1 for parameter values). An extra segment of 1.6 kg was attached to the forearms to represent the object to be lifted. All segments were connected with frictionless hinge joints. The position and orientation of the feet were fixed during the entire simulation. This constraint did not lead to unrealistic situations in any of the simulations. Parameter values for the skeletal model were derived on the basis of the anthropometrical measurements of the subject whose lifting movement was simulated (see below) (Plagenhoef et al. 1983).

**Table 1** Segment parameter values

| | $l$ (cm) | $d$ (cm) | $m$ (kg) | $J$ (kg·m$^2$) |
|---|---|---|---|---|
| Feet | 13.3 | 6.6 | 2.00 | 0.088 |
| Lower legs | 43.2 | 24.5 | 6.67 | 0.121 |
| Upper legs | 39.0 | 22.1 | 14.74 | 0.245 |
| Pelvis | 13.2 | 4.8 | 5.56 | 0.220 |
| Trunk+head | 49.8 | 35.7 | 33.72 | 2.122 |
| Upper arms | 33.4 | 14.5 | 4.56 | 0.050 |
| Fore arms | 35.2 | 15.5 | 3.54 | 0.040 |

$l$ = length; $d$ = distance from proximal joint in chain of segments to center of gravity; $m$ = mass; $J$ = moment of inertia (relative to center of gravity). Note that $m$ and $J$ are summed for left and right parts of the human body

The skeletal model was actuated by seventeen "muscles": m. tibialis anterior, m. soleus, m. gastrocnemius, mm. vastii, m. rectus femoris, m. biceps femoris (mono and biarticular), m. glutaeus maximus, m. iliopsoas, m. erector spinae, m. rectus abdominus, posterior m. deltoid, anterior m. deltoid, m. brachialis, m. triceps brevis, m. triceps longus and caput longum of m. biceps brachii. These "muscles" are described by a Hill-type muscle model consisting of a contractile element CE, an elastic element PEE in parallel to this CE, and a series elastic element SEE. As in none of the simulations a muscle was stretched to the extent that PEE delivered any force, its behavior will not be discussed further. Behavior of SEE and CE are outlined in Fig. 2; some of the abbreviations used there are defined in the following paragraph.

The flow of calculations is schematically represented in Fig. 3. Functions $f_1$ and $f_2$ together describe a non-linear first order system linking active state ($q$) (Ebashi and Endo 1968 ) to stimulation, the one-dimensional input of the single muscle (STIM), as proposed by Hatze (1981b). In this model of activation dynamics, $q$ also depends on contractile element length ($L_{CE}$), to reflect the length-dependent [$Ca^{2+}$] sensitivity (Fig. 2d). Function $f_3$ represents the Hill force–velocity relationship (Fig. 2c), formulated such that the contractile element velocity ($V_{CE}$) is calculated from $L_{CE}$, $q$, and contractile element force ($F_{CE}$), which in absence of PEE force, equals series elastic element force ($F_{SE}$). $F_{SE}$ is calculated in $f_5$ from series elastic element length ($L_{SE}$), which is modelled as a quadratic spring (see Fig. 2a). $L_{SE}$ in turn is calculated in $f_4$ as the difference between muscle–tendon complex length ($L_{MTC}$) and $L_{CE}$.

Polynomial relations are used in function $f_4$ to calculate $L_{MTC}$ from the joint angles: for monoarticular muscles, $L_{MTC}$ is given by: $A_0 + A_1 \cdot \phi + A_2 \cdot \phi^2$, where $\phi$ is the angle of the joint that is spanned by the muscle (defined as the difference between adjacent segment angles), $A_0$ is the length of $L_{MTC}$ when the joint is fully stretched, and $A_1$ and $A_2$ are coefficients that were obtained using the tendon excursion method (Grieve et al. 1978); for biarticular muscles, $L_{MTC}$ depends on two joint angles: $A_0 + A_{1,1} \cdot \phi_1 + A_{2,1} \cdot \phi_1^2 + A_{1,2} \cdot \phi_2 + A_{2,2} \cdot \phi_2^2$. Finally, $f_6$ transforms the muscle forces in their contributions to net joint moments ($M$), using moment arms that follow from the same polynomial relations. Together with the gravitational forces, these net joint moments determine the angular accelerations of the segments ($\ddot{\varphi}$) (as well as the reaction forces) in $f_7$. The Newtonian equations of motion in $f_7$ are automatically derived using MUSK (Casius 1995; Casius et al. 2004). For the complete open-loop system as presented in Fig. 2, the state vector has dimension 48 (7 segment angles $\varphi$, 7 segment angular velocities $\dot{\varphi}$, 17 [$Ca^{2+}$] concentrations $\gamma$, and 17 contractile element lengths $L_{CE}$). Values for muscle-specific parameters are presented in Table 2.

## 2.2 Calculating the input signals

Before perturbed lifting simulations could be performed, control signals had to be calculated for both models. In the absence of a perturbation, these signals had to result in a whole body lifting movement that closely resembled experimental data concerning lifting a crate of 1.6 kg, which was placed 0.25 m above floor level, with an intermediate lifting technique at a self-chosen, non-maximal velocity (van der Burg et al. 2000; van der Burg and van Dieën 2001b). The average movement of all eight unperturbed trials of the subject that had the lowest residual forces after calculating inverse dynamics (de Looze et al. 1992) among the whole group of ten subjects was used as the unperturbed experimental lifting movement. This guaranteed that data of the most adequately modelled subject was chosen. During real-life experiments, mass perturbations of 10 kg were applied. The mass was added before lift-off, or the mass was added when the crate in which the mass was placed, was lifted 10 cm. These results were used to check whether the results of the simulation were realistic.

An optimization was performed to find a STIM-pattern that resulted in a movement, which closely resembled the unperturbed experimental lifting movement. In the optimization, the sum of squared differences between the experimental and simulated segment angles (SSD) was calculated at regular intervals (50 Hz). The maximum SSD during the entire movement was used as the cost function value for the trial STIM-pattern in question, and the goal of the optimization was to minimize this value.

In order to reduce the complexity of the optimization problem to be solved, the following constraints were imposed on the STIM-pattern. Primarily, it was decided to consider only the first 300 ms after the perturbation as feedback control was expected to have definitely taken over by that time. Then, we assumed that only the STIM levels of the monoarticular agonist muscles (i.e., m. soleus, mm. vastii, m. biceps femoris (monoarticular), m. glutaeus maximus, m. erector spinae, anterior m. deltoid, m. brachialis) were modulated during the simulation. The STIM levels of the antagonist muscles and of the biarticular muscles were set such that the active state $q$ of these muscles was initially 0.20, as preliminary analysis showed that this level was necessary in the elbow to prevent unrealistic arm movements during perturbed lifting. This value of $q$ resulted in an average STIM-level of 7% for the antagonist and biarticular muscles (see discussion). Finally, the STIMs of the monoarticular agonist mus-

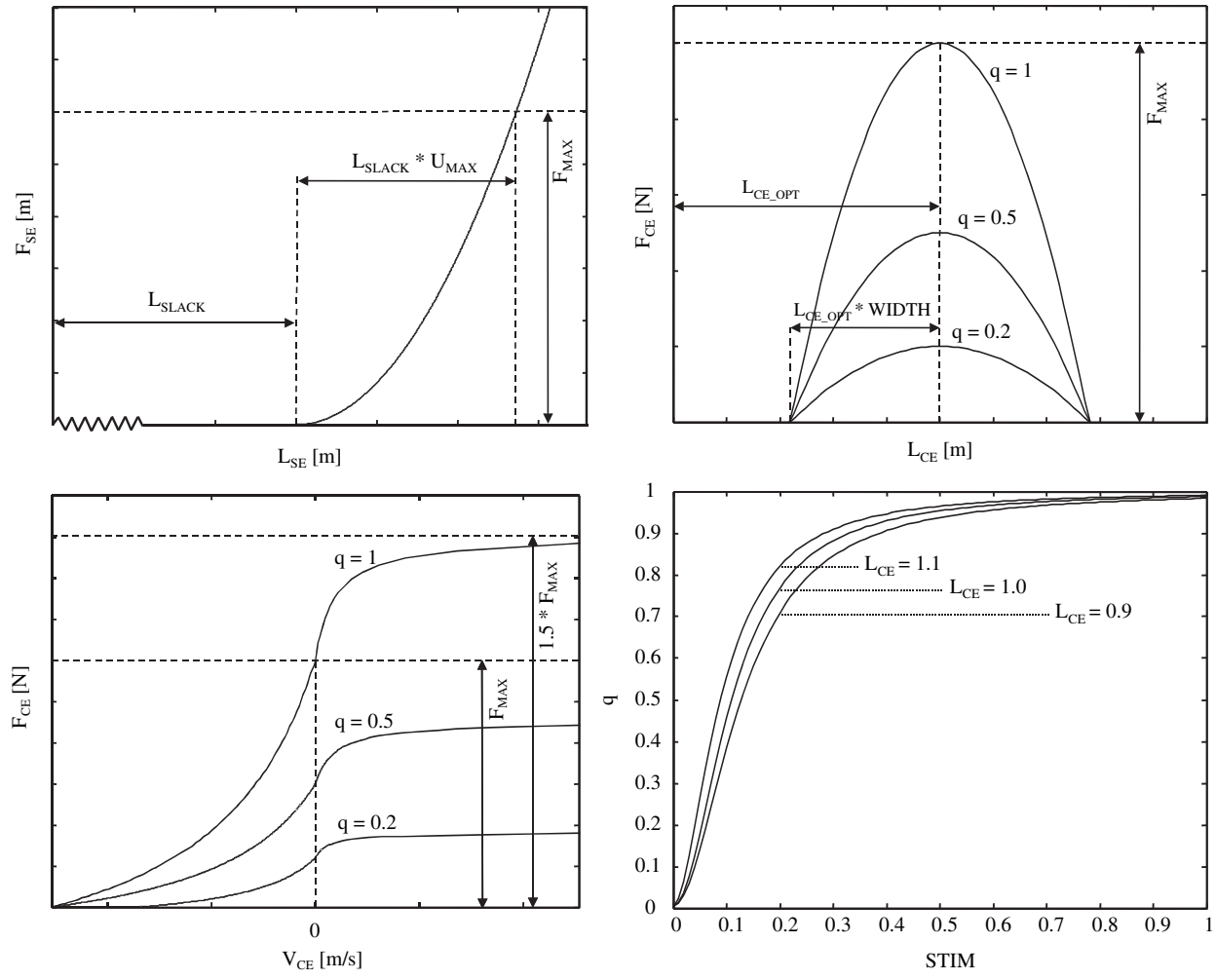


**Fig. 2** Relationships describing the behavior of SEE and CE. Muscle-specific parameters are listed in Table 2. Note that, roughly speaking; active state $q$ acts as a scaling factor for force in the force–length and force–velocity curves of the CE. For justification and a more elaborate description of the described relationships we refer to van Soest and Bobbert (1993). *Top-left* **a** SEE force–length relation. In this study, the force–length behavior of the SEE is governed by a second order polynomial. Parameters describing this polynomial are (1) $F_{\mathrm{MAX}}$ [N], the maximal isometric force, (2) $L_{\mathrm{SLACK}}$ [m], the maximum length at which force equals zero, and (3) $U_{\mathrm{MAX}}$ (dimensionless), the relative elongation at maximal isometric force, which was set to 0.04 for all muscles in this study, based on quick-release experiments on animal preparations (Ettema and Huijing 1989). *Top-right* **b** CE force–length relation. The CE force–length curve is also described by a second order polynomial. Parameters describing this polynomial are (1) $F_{\mathrm{MAX}}$ [N], the maximal isometric force, (2) $L_{\mathrm{CE_0PT}}$ [m], the length at which the maximal isometric force is delivered, and (3) width (dimensionless), which was set to 0.56 for all muscles in this study, based on a least squares fit to the force–length relationship of human sacromeres. *Bottom-left* **c** CE force–velocity relation ($L_{\mathrm{CE}} = 1$). The concentric force–velocity curve (i.e., $V_{\mathrm{CE}} \leq 0$) is based on the description first given by Hill (1938) and extended in order to accommodate the influence of $L_{\mathrm{CE}}$ and $q$. The eccentric force-velocity curve (i.e. $V_{\mathrm{CE}} \geq 0$) is described by a hyperbolic function, which approaches 1.5 $F_{\mathrm{MAX}}$ as eccentric velocity goes to infinity. At $V_{\mathrm{CE}} = 0$, the slope of the eccentric force-velocity curve is twice the slope of the concentric force–velocity curve. For exact formulas and parameter values of the concentric and eccentric force–velocity curves see van Soest and Bobbert (1993). *Bottom-right* **d** CE $q$-STIM relation, showing the effect of the length-dependent $[Ca^{2+}]$ sensitivity on active state $q$ for three different CE lengths [relative to $L_{\mathrm{CE\_OPT}}$ (Hatze 1981a)]. Note that length-dependent $[Ca^{2+}]$ sensitivity is largest between STIM = 0.1 and STIM = 0.3

cles were allowed to change only once within the time simulated, as preliminary work had indicated that this was sufficient to closely resemble the experimental movements. These constraints reduced the optimization problem in finding the time-onset (in the range of 0–300 ms) and stimulation level (in the range of 0–1) for the six monoarticular agonist muscles. The optimization problem was solved using a parallel genetic algorithm (van Soest and Casius 2003).

The net joint moments as a function of time that resulted from a simulation with this STIM-pattern were used as the control signals for the MOM-model. Thus, apart from negligible numerical errors, the two models produce identical output for the unperturbed movement. In the case of a perturbation, however, moments in the MOM-model will not change, whereas moments in the STIM-model will change due to force-length-velocity characteristics of muscles. The

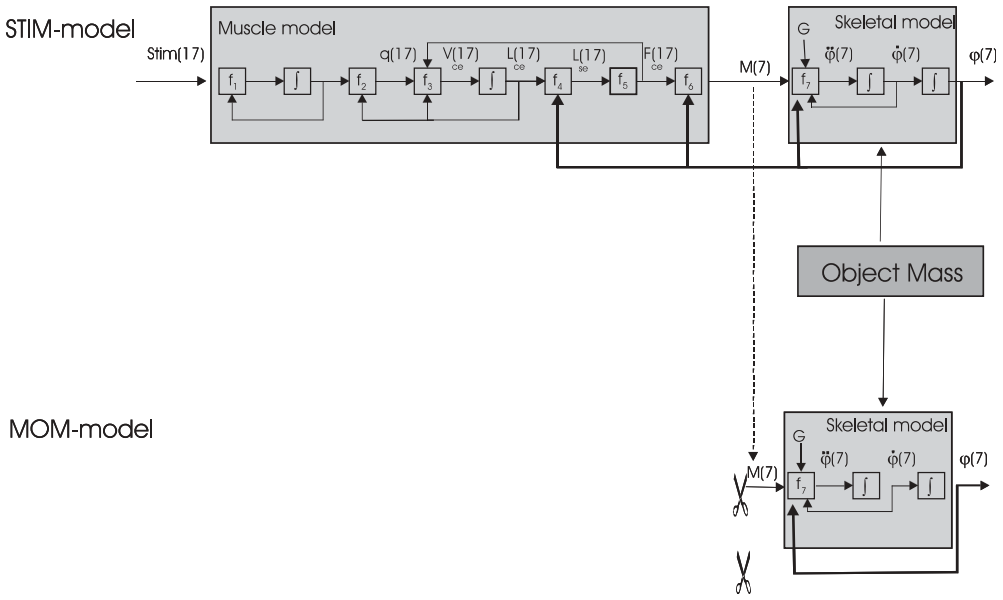


**Fig. 3** *Block diagrams* showing the flow of calculations in both simulation models (upper diagram STIM-model, lower diagram MOM-model). M(7) is in unperturbed condition, the same for the STIM- and MOM-models. As can be derived from the diagrams, changes in objects mass alter M(7) only in the STIM-model due to the loops that are present. *Numbers in parentheses* represent the dimensions of the juxtaposed variable. See text for details on blocks $f_1$ through $f_7$. *Blocks* containing the integral sign indicate integration with respect to time. *G* represents the gravitational force

**Table 2** Muscle parameter values

| | $L_{ce_o}pt$(m) | $F_{max}$(N) | $L_{slack}$(m) | $d_{ankle}$(m) | $d_{knee}$(m) | $d_{hip}$(m) | $d_{L5-S1}$(m) | $d_{shoulder}$(m) | $d_{elbow}$(m) |
|---|---|---|---|---|---|---|---|---|---|
| m. tibialis anterior | 0.087 | 2400 | 0.31 | 0.0372 | | | | | |
| m. soleus | 0.055 | 6000 | 0.246 | 0.0345 | | | | | |
| m. biceps femoris (monoarticular) | 0.1328 | 1000 | 0.1 | | 0.026 | | | | |
| m. vastii | 0.093 | 10500 | 0.17 | | 0.042 | | | | |
| m. glutaeus maximus | 0.2 | 5500 | 0.15 | | | 0.062 | | | |
| m. iliopsoas | 0.102 | 8000 | 0.115 | | | 0.05 | | | |
| m. erector spinae | 0.17 | 7000 | 0.05 | | | | 0.0530 | | |
| m. rectus abdominus* | 0.18 | 1500 | 0.07 | | | | 0.075 | | |
| anterior m. deltoid | 0.1337 | 3440 | 0.0329 | | | | | 0.03 | |
| posterior m. deltoid | 0.1397 | 3150 | 0.0489 | | | | | 0.03 | |
| m. brachialis * | 0.085 | 3300 | 0.054 | | | | | | 0.0164 |
| m. triceps brevis* | 0.093 | 2660 | 0.054 | | | | | | 0.0264 |
| m. gastrocnemius* | 0.055 | 3000 | 0.382 | 0.0345 | 0.0135 | | | | |
| m. rectus femoris | 0.081 | 3500 | 0.340 | | 0.042 | 0.035 | | | |
| m. biceps femoris (biarticular) | 0.104 | 4400 | 0.370 | | 0.026 | 0.077 | | | |
| m. biceps brachii caput longum* | 0.0905 | 930 | 0.0315 | | | | | 0.03 | 0.0214 |
| m. triceps longus* | 0.127 | 980 | 0.213 | | | | | 0.03 | 0.0264 |

$L_{ce_o}pt$ = optimal length of contractile element; $F_{max}$ = maximal isometric force of contractile element (summed for left and right parts of the human body); $L_{slack}$ = slack length of series elastic element; $d_{ankle}, \ldots, d_{elbow}$ = moment arm over joint considered. Moment arms of muscles that depend on joint angle (marked with *) are averaged over start position (time = 0 s) and end position (time=0.300 s) of the reference movement. Parameter values for the leg muscles are the same as in van Soest and Casius (2000), where they proved to be highly accurate in predicting the maximum power output in a sprint-cycling task. These parameters were originally used in van Soest and Bobbert (1993), and are based on measurements in a single set of cadavers. For the arm muscles, the values used in Welter and Bobbert (2002) were taken, because this set also has proven to result in a behavior that was comparable to experimental data. These parameters were based on the work by Murray et al. (2000), and C.W. Spoor (personal communication). Unfortunately, the wrong values have been reported in Welter and Bobbert (2002); the values listed here are the correct ones (T. Welter, personal communication). Finally, the values for the trunk muscles were derived from Thorstensson and Nilsson (1982), McGill (1996), and Andersson et al. (1988), and the relation between joint angle and joint moment predicted from these parameters were in good agreement with the data we collected for a single subject on a isokenetic KinCom (KinCom H500, Chattecx, Chattenooga, TE)

difference between the behavior of both models in the perturbed condition reflects the effect of force-length-velocity characteristics.

The simulation was started at the instant the vertical velocity of the hand in the experimental trial became positive (upward). In the simulation, the initial state vector was chosen as follows: initial values for the segment angles and angular velocities were set identical to the experimental values; initial STIMs and state variables for the muscles were set assuming steady-state equilibrium. Given the initial STIMs for the antagonists and the biarticular muscles, the initial STIMs for the monoarticular muscles were set such that the net joint moments resulted in segment angular accelerations that exactly matched those found in the experimental trial.

### 2.3 Simulations

In order to assess the factors underlying the perturbation resistance of the lifting movement, 10 kg mass perturbations were applied to the lifting movement for all four models (STIM-model with fixed elbow, STIM-model with free elbow, MOM-model with fixed elbow, and MOM-model with free elbow). In these simulations, the input signals were those that were identified previously; that is, the input signals were not altered in response to the perturbations (Fig. 2). First, an instantaneous increase of crate mass of 10 kg was applied (at the start of the simulation). Second, the same mass perturbation was applied 70 ms after lift-off, when the vertical velocity of the crate was about 0.2 m/s, which was in close correspondence with the experimental data (van der Burg and van Dieën 2001a, b). The lifting movements that resulted from the perturbed 10 kg simulations before and after lift-off in the STIM-model with free elbow and in the MOM with fixed elbow, were compared to the 10 kg-perturbed lifting movements of all ten subjects in the real-life experiment. The 5th and 95th percentiles of the lifting movements for each perturbation condition separately (before and after lift-off), based on the values of all subjects were considered to represent the normal range of variability.

## 3 Results

In the absence of a perturbation, the simulation closely resembled the experimental data. The maximum cost function value SSD in the optimal solution was 0.14 $deg^2$ : No segment angle in the unperturbed condition deviated more than 0.37° from the experimental data concerning lifting of the 1.6 kg crate. As intended, this also applied for the segment angles in the MOM-model. When the perturbation was applied, the deviations from the experimental perturbed data increased in the STIM-model with free elbow. The curves of the trunk angle were just within the normal range of variation of the experimental data, when the perturbation was applied before, as well as after lift-off (Fig. 4).

The linear and angular momenta of the trunk before lift-off were not sufficient to resist the perturbation. When the perturbation was applied in the MOM-model with fixed elbow, thereby excluding the effect of elbow motion and of the force-length-velocity characteristics, the curves of the trunk angles deviated outside the normal range of variation of the experimental data (Fig. 4).

Allowing extension of the elbow increased the resistance of the trunk to perturbations, (Fig. 5). When the elbow was fixed, the deviations of the trunk were larger compared to the trunk deviations when the elbow was not fixed in the MOM-model as well as in the STIM-model for both perturbations (Fig. 5). However, the effects of fixation of the elbow were larger in MOM than in the STIM-model, indicating an interaction between the effect of elbow motion and the effect of force-length-velocity characteristics of muscles. Closer examination revealed that the extension of the elbow due to the extra-added mass was small in the STIM-model (Fig. 6), corresponding to the experimental data. The small effect of the extra-added mass on the elbow extension is caused likely by the perturbation resistance effect of the force-length-velocity characteristic of muscles spanning the elbow joint. When the elbow joint had no rotational stiffness, as is the case in the MOM-model, the elbow extension due to the extra-added mass was much larger (Fig. 6). Consequently, the effect of passive extension of the elbow to the resistance of the trunk to perturbations was also much larger in the MOM-model, as was indicated by a decreased angular deviation with a free elbow (Fig. 5).

The effect of adding force-length-velocity characteristics of muscles to the model differed depending on the movement that was allowed in the elbow. When no elbow movements were allowed (= fixed elbow), adding force-length-velocity characteristics of muscles to the model increased the initial resistance of the trunk to perturbations (Fig. 5). In contrast, when the elbow was free to move, adding force-length-velocity characteristics decreased the initial resistance to perturbation (Fig. 5). The force-length-velocity characteristics of muscles stabilized the elbow joint in the STIM-model with free elbow, and thus less elbow extension occurred (Fig. 6). Consequently, the trunk angle was more perturbed compared to the MOM-model with free elbow, in which the elbow had no rotational stiffness.

## 4 Discussion

The initial perturbation resistance of the trunk in perturbed lifting movements, as observed experimentally, could not be explained by the momentum effect of the trunk alone as is showed by the results of the MOM-model with fixed elbow. Although the trunk has a high inertia, the linear and angular momenta of the trunk before lift-off were not sufficient to resist the perturbation. Adding force-length-velocity characteristics of muscles to the model improved the resistance of the trunk to perturbations. Allowing extension of the elbows helps to postpone the perturbation of the trunk. While the

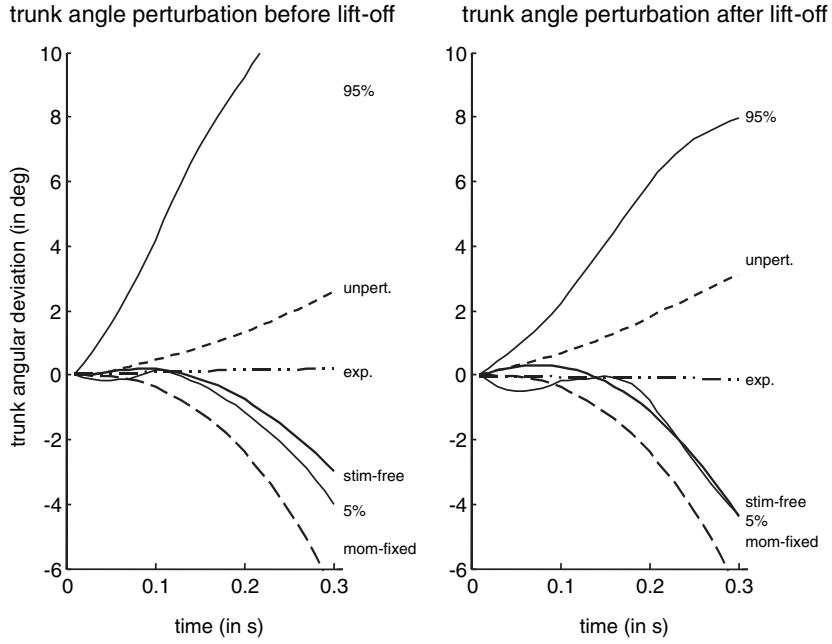


**Fig. 4** Time series of the trunk angular deviation after a 10 kg perturbation relative to the start position. Time zero is the instant of which the perturbation was applied. The *left panels* represent the perturbations before lift-off, the *right panels*, the perturbations after lift-off. The solid *thick line* represents the simulation data of the STIM-model with free elbow. The unperturbed trial is represented by a *dashed line*. The perturbed trial of the subject on which the simulation is based, is represented by the *dashed-dotted line*. The 5th and 95th percentiles of perturbed experimental data of all subjects are represented by the thin *lines*. The long *dashed line* represents the simulation data of the MOM-model with fixed elbow

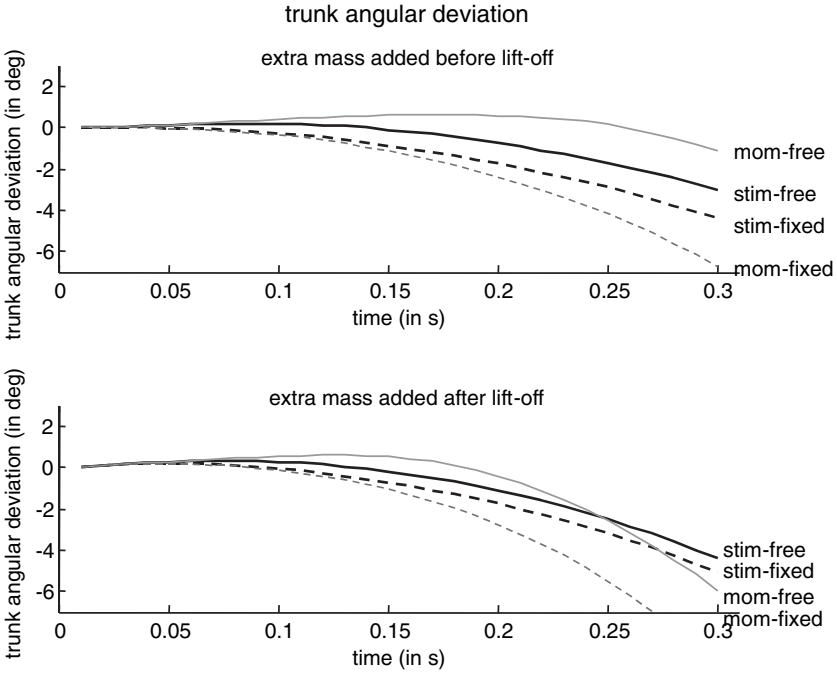


**Fig. 5** Time series, showing the effect on trunk angle of allowing a passive elbow extension after a 10 kg perturbation in the STIM-model with free elbow and the MOM-model with free elbow. The *upper panel* represents the perturbation before lift-off, and the *lower panel* represents the perturbation after lift-off. Time zero is the instant at which the perturbation was applied. The *solid lines* represent the model in which elbow extension was allowed, and the *dashed lines* the model in which the elbow was fixed. The *thin lines* represents the MOM-model and the *thick lines* the STIM-model

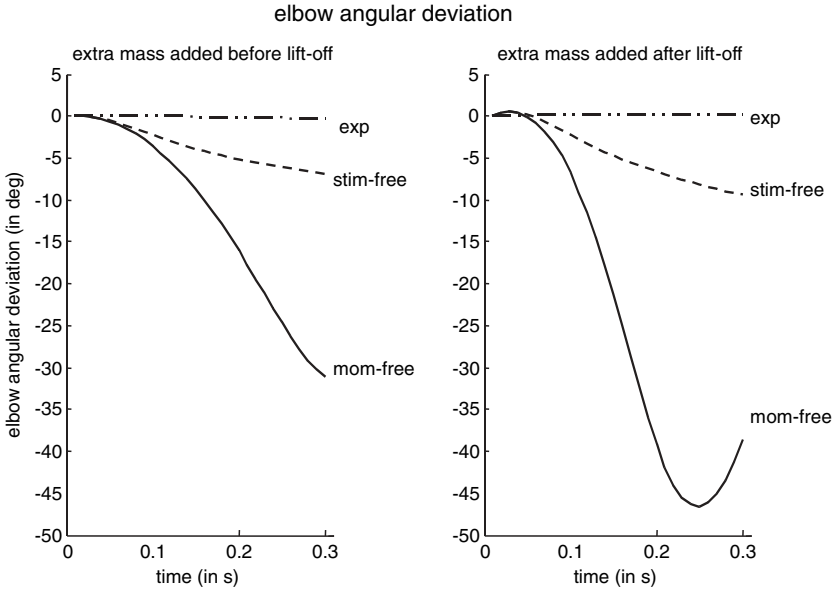


**Fig. 6** Time series of the elbow angular deviation after a 10 kg perturbation. The *left panel* represents the perturbation before lift-off, the *right panel* the perturbation after lift-off. Time zero is the instant at which the perturbation was applied. The *dashed line* represents the STIM-model, and the *solid line* the MOM-model. The perturbed trial of the subject of which the simulation is based, is represented by the *dashed-dotted line*

elbows extend, perturbation is not fully apparent at the trunk. The delay until the full perturbation is experienced at the shoulder compared to the immediate sensation in the arms, might allow adaptations in trunk muscle stimulation to prevent substantial deviations of the trunk movement (Hodges et al. 1999). However, higher elbow stiffness attenuated this effect as can be appreciated from a comparison of the STIM-model with free elbow to the MOM-model with free elbow. Higher elbow stiffness decreased the downward acceleration of the forearm, so that the load will be quickly apparent at the shoulder. A faster propagation of the load to the trunk will decrease the time left for active responses of trunk muscles. Consequently, it is to be expected that when a lifting movement is performed with stiff or extended elbows, trunk movement will be more affected after a perturbation. This may increase injury risk, since sudden movements are associated with injury of the lower back (Magora 1973; Manning et al. 1984).

The fact that due to the perturbation, the trunk is flexing instead of extending in the simulations, suggests that active responses are required to fully compensate for the perturbation. Although the three described effects could postpone the need for active muscle responses, active responses are required to fully compensate the perturbation effects. Indeed, in the experimental data an increase in muscle activity was seen approximately 100 ms after lift-off of a load that was unexpectedly heavy by 10 kg (van der Burg et al. 2000; van der Burg and van Dieën 2001b).

It was found that the effects of the force-length-velocity characteristics could be present to a greater extent in real-life. In the simulations, the stimulation level of only a small number of muscles was adapted during the simulation. Furthermore, the stimulation of these muscles was allowed to change only once. A less restrictive stimulus pattern could enhance the contribution of force-length-velocity characteristics. Including other muscle characteristics to our model, such as short-range stiffness and history dependence, may further increase the resistance to perturbation (Stokes et al. 2000; Ettema 2002).

The force-length-velocity characteristics of muscles increase the resistance of the trunk to perturbation due to three independent mechanisms. First, the force–velocity relation of the CE is described by a monotonous increasing function (van Soest and Bobbert 1993). This implies that, for a given neural input, a muscle that is stretching or is contracting more slowly will produce more force and thereby oppose the perturbation. Second, the isometric force–length relation of the CE that results from myofilamentary overlap, is modeled as a parabolic function with a maximum at the point where CE is at its optimum length (Fig. 1b). Flexion of the trunk will increase $L_{CE}$ of the trunk extensors and decrease $L_{CE}$ of the trunk flexors. Given the parabolic function, lengthening of a muscle that is below the optimum length will result in an increased muscle force, while shortening will result in a decreased muscle force. Therefore, extensor muscle force will increase if $L_{CE}$ is below optimum length and decrease if $L_{CE}$ is above optimum length. For flexor muscle force, the opposite holds. Thus, ideally, all muscles spanning the lumbar-sacral joint should have a relatively short $L_{CE}$ to counteract trunk flexion. Initially, $L_{CE}$ of most trunk muscles is indeed below the optimum length in simulations performed in this study. Third, the length-dependent $[Ca^{2+}]$ sensitivity also reduces the effect of perturbation. The active state of stretching muscles increases, and the active state of shortening mus-

cles decreases without adaptation of STIM (Kistemaker et al. 2005, in press). Thus, the force output of agonist muscles increases after a perturbation, whereas the force output of the antagonist muscles decreases.

The level of co-contraction influences the effects of force-length-velocity characteristics in resisting a perturbation. In this study, STIMs concerning co-activation varied from 3 to 11% of the maximum stimulation. This level of co-activation, corresponding with $q = 0.2$, was only necessary in the elbow muscles, and not in the muscles spanning other joints, to mimic the experimental data. However, to simplify the model, we used a constant activation level for all antagonistic and biarticular muscles. Besides, the level of trunk co-activation used in the simulation was realistic, as in experimental EMG-data, the level of trunk co-activation varied from 2 to 24% in lifting (Granata et al. 1997; de Looze et al. 2000; van der Burg and van Dieën 2001b).

## 5 Conclusion

In addition to the momentum of the trunk, the force-length-velocity characteristics of muscles are necessary to account for the perturbation resistance of trunk movements as found experimentally. Initial extension of the elbow due to the mass perturbation can delay the propagation of the load to the shoulder. However, this delay is reduced due to the impedance at the elbow provided by the muscle characteristics around the elbow.

## References


Andersson E, Sward L, Thorstensson A (1988) Trunk muscle strength in athletes. Med Sci Sports Exerc 20(6):587–593

Casius LJR (1995) MUSK: a software system that supports computer simulations of large-scale realistic models of the neuro-musculoskeletal system. Faculty of Human Movement Sciences, Vrije Universiteit, Amsterdam, pp 6–50

Casius LJR, Bobbert MF, Soest AJv (2004) Forward dynamics of two-dimensional skeletal models. A Newton-Euler approach. J Appl Biom 20:421–449

de Looze MP, Bussmann JBJ, Kingma I, Toussaint HM (1992) Validation of a dynamic linked segment model to calculate joint moments in lifting. Clin Biomech 7:161–169

de Looze MP, Boeken-Kruger MC, Steenhuizen S, Baten CT, Kingma I, van Dieën JH (2000) Trunk muscle activation and low back loading in lifting in the absence of load knowledge. Ergonomics 43(3):333–344

Ebashi S, Endo M (1968) Calcium ion and muscular contraction. Prog Biophys Mol Biol 18:123–183

Ettema GJ (2002) Effects of contraction history on control and stability in explosive actions. J Electromyogr Kinesiol 12(6):455–461

Ettema GJ, Huijing PA (1989) Properties of the tendinous structures and series elastic component of EDL muscle-tendon complex of the rat. J Biomech 22(11–12):1209–1215

Granata KP, Marras WS, Davis KG (1997) Biomechanical assessment of lifting dynamics, muscle-activity and spinal loads while using 3 different styles of lifting belt. Clin Biomech 12(2):107–115

Grieve DW, Pheasant S, Cavanagh PR (1978) Prediction of gastrocnemius length from knee and ankle joint posture. In: Biomechanics VI-A. University Park Press, Baltimore, USA, pp 405–412

Hatze H (1981a) The use of optimally regularized fourier series for estimating higher-order derivatives of noisy biomechanical data. J Biomech 14:13–18

Hatze H (1981b) Myocybernetic control models of skeletal muscle: characteristics and applications. University of South Africa, Pretoria, pp 28–41

Hill AV (1938) The heat of shortening and the dynamic constants of muscle. Proc Royal Soc 126B:136–195

Hodges P, Cresswell A, Thorstensson A (1999) Preparatory trunk motion accompanies rapid upper limb movement. Exp Brain Res 124(1):69–79

Kistemaker DA, Van Soest AJ, Van Soest AJ, Bobbert MF, Length-dependent [Ca2+] sensitivity adds stiffness to muscle. J Biomech (in press)

Magora A (1973) Investigation of the relation between low back pain and occupation, part IV. Physical requirements: bending, rotation, reaching and sudden maximal effort. Scand J Rehabil Med 5:186–190

Manning DP, Mitchell RG, Blanchfield LP (1984) Body movements and events contributing to accidental and nonaccidental back injuries. Spine 9(7):734–739

McGill SM (1996) A revised anatomical model of the abdominal musculature for torso flexion efforts. J Biomech 29(7):973–977

Murray WM, Buchanan TS, Delp SL (2000) The isometric functional capicity of muscles that cross the elbow. J Biomech 33(8):943–952

Nijhof E, Kouwenhoven E, (eds) Simulation of multijoint arm movements. Biomechanics and neural control of posture and movement. Springer, Berlin Heidelberg New York, pp 363–372

Plagenhoef S, Evans FG, Abdelnour T (1983) Anatomical data for analyzing human motion. Res Q Exerc Sport 54(2):169–178

Seyfarth A, Gunther M, Blickhan R (2001) Stable operation of an elastic three-segment leg. Biol Cybern 84(5):365–382

Stienen GJ, Blange T, Treijtel BW (1985) Tension development and calcium sensitivity in skinned muscle fibres of the frog. Pflugers Arch 405(1):19–23

Stokes IA, Gardner-Morse M, Henry SM, Badger GJ (2000) Decrease in trunk muscular response to perturbation with preactivation of lumbar spinal musculature. Spine 25(15):1957–1964

Thorstensson A, Nilsson J (1982) Trunk muscle strength during constant velocity movements. Scand J Rehabil Med 14(2):61–68

van der Burg JCE, van Dieën JH (2001a) The effect of timing of a perturbation on the execution of a lifting movement. Hum Mov Sci 20(3):243–255

van der Burg JCE, van Dieën JH (2001b) Underestimation of object mass in lifting does not increase the load on the low back. J Biomech 34(11):1447–1453

van der Burg JCE, van Dieën JH, Toussaint HM (2000) Lifting an unexpectedly heavy object: the effects on low-back loading and balance loss. Clin Biomech 15(7):469–477

van Dieën JH, Thissen C, van de Ven A, Toussaint HM (1991) The electro-mechanical delay of the erector spinae muscle: influence of rate of force development, fatigue and electrode location. European J Appl Physiol 63:216–222

van Soest AJ, Bobbert MF (1993) The contribution of muscle properties in the control of explosive movements. Biol Cybern 69(3):195–204

van Soest AJ, Casius LJR (2000) Which factors determine the optimal pedaling rate in sprint cycling? Med Sci Sports Exerc 32(11):1927–1934

van Soest AJ, Casius LJR (2003) The merits of a parallel genetic algorithm in solving hard optimization problems. J Biomech Eng 125:141–146

van Soest AJ, Schwab AL, Bobbert MF, Ingen Schenau GJv (1993) The influence of the biarticularity of the gastrocnemius muscle on vertical-jumping achievement. J Biomech 26(1):1–8

Wagner H, Blickhan R (2003) Stabilizing function of antagonistic neuromusculoskeletal systems: an analytical investigation. Biol Cybern 89(1):71–79

Welter TG, Bobbert MF (2002) Initial arm muscle activation in a planar ballistic arm movement with varying external force directions: a simulation study. Motor Control 6(3):217–229